Available online at www.sciencedirect.com
ScienceDirect
European Journal of Mechanics B/Fluids 27 (2008) 131–149

Particle grouping in oscillating flows

Sergei Sazhin [a,*], Tal Shakked [b], Vladimir Sobolev [c], David Katoshevski [b]

[a] *School of Engineering, Faculty of Science and Engineering, The University of Brighton, Brighton BN2 4GJ, UK*
[b] *Department of Biotechnology and Environmental Engineering, Ben-Gurion University of the Negev, Beer-Sheva 84105, Israel*
[c] *Department of Differential Equations and Control Theory, Samara State University, Akademika Pavlova Street 1, Samara 443011, Russia*

Received 8 August 2006; received in revised form 16 April 2007; accepted 19 April 2007

Available online 29 April 2007

Abstract

An equation describing the dynamics of spherical particles in an oscillating Stokesian flow in the frame of reference moving with the phase velocity of the wave, and only taking into account the contribution of the drag force, is simplified in two limiting cases. Firstly, the case when Stokes numbers are small is considered. Secondly, the analysis focuses on the case when the initial location of the particles is close to the location where the particles are grouped (their velocities and accelerations in the wave frame of reference are equal to zero), $x_{\lim}$. This is followed by an analysis of the dynamics of non-Stokesian particles. In all cases, the analytical results are validated against the results of numerical solution of the equation of particle motion. Three types of trajectories are predicted when particles approach $x_{\lim}$: the trajectories describing the monotonic approach to $x_{\lim}$, the trajectories describing the approach to $x_{\lim}$ with oscillations and trajectories repelled from $x_{\lim}$. These are identified with stable nodes, stable foci and saddles. The trajectories in the zone between stable nodes and foci are identified as stable stars. Using Dulac's criterion, it is pointed out that none of the particle trajectories in the position–velocity plane can be closed. This result is illustrated by the trajectories calculated using the numerical solution of the equation for particle dynamics for various parameter values.

Keywords: Spray; Stokesian flow; Clustering

1. Introduction

The problem of calculating droplet and particle trajectories in various flow structures has been discussed in numerous papers (e.g. [1–3] and the references therein). This problem is challenging from the point of view of mathematical analysis and important for various engineering, environmental and medical applications including those related to modelling of dynamics of atmospheric particles [4,5], modelling of inhaled particles [6], exhaust Diesel particles filtration [7], modelling of sprays in internal combustion engines [8,9] and other applications [10,11]. To understand the underlying physics of the phenomenon, it is often useful to simplify the problem, while retaining its non-trivial features. This approach was adopted in [12]. These authors studied the process of grouping of non-evaporating particles based on a simple 1D model. The analysis was performed in a stationary frame of reference, and effects of particles on gas were ignored. Although the assumptions of this model might seem to be too simplistic for direct practical

* Corresponding author.
E-mail address: S.Sazhin@brighton.ac.uk (S. Sazhin).

0997-7546/$ – see front matter
doi:10.1016/j.euromechflu.2007.04.003

engineering applications, they allowed the authors to get a clear picture of the effect of the oscillating gas flow on droplet grouping. This could potentially complement the results predicted by more advanced DNS and LES models (e.g. [13]).

The main limitation of the analysis performed by [12] is that it was based on the numerical solution of the equation of particle motion. Although this approach allowed the authors to establish some new features of particle behaviour (grouping and non-grouping) many underlying physical properties of this behaviour remained unclear. In this paper, the analysis by [12] is extended in two main directions. Firstly, we restricted ourselves to the Stokesian approximation (small Reynolds numbers). In this case, the analysis of the equation of particle motion is performed in some limiting cases using analytical methods, allowing us to get a much clearer understanding of the physics of the phenomenon. Results of this analysis are compared with the results of numerical simulation where appropriate. Secondly, the case of arbitrary particle Reynolds numbers (non-Stokesian flow) is considered. The general properties of the equation of particle motion are investigated and particle trajectories are calculated numerically. Some properties of these trajectories are compared with those which follow from the simplified theoretical analysis of Stokesian trajectories. The range of possible applications of the results is the same as discussed in [12].

Basic equations of the model and approximations are presented and discussed in Section 2. In Section 3, analytical solutions of these equations for small Stokes numbers are shown and discussed. The focus of Section 4 is on converging and repelling trajectories of particles during the process of their grouping for arbitrary Stokes numbers, provided that the Stokesian approximation remains valid. In Section 5, some analytical results obtained in Sections 3 and 4 are compared with the results of numerical analysis of Stokesian trajectories. In Section 6, non-Stokesian particle trajectories are investigated using numerical approach. The properties of these trajectories are related to some analytical results where appropriate. The main results of the paper are summarised in Section 7.

2. Basic equations and approximations

Let us consider a two-dimensional incompressible flow described by the following velocity field:

$$\mathbf{v}(x, y, t) = \big(V_a - V_b \sin(kx - \omega t)\big)\mathbf{i}_x + \big(yV_b k \cos(kx - \omega t)\big)\mathbf{i}_y \tag{1}$$

where $\mathbf{v}(x, y, t)$ is the dimensional gas flow velocity at a time t at a location (x, y), V_a is the dimensional mean flow velocity, V_b is the dimensional amplitude of the velocity oscillation in the x-direction, k is the wave number and ω is the angular velocity. Without loss of generality we assume that V_a and V_b are positive. The flow, described by Eq. (1), has a period $\lambda = 2\pi/k$ along the x-axis (wave length) and a time period $T = 2\pi/\omega$. The dimensional phase velocity of the wave is $V_\omega = \omega/k$.

The flow described by Eq. (1) satisfies the continuity equation.

For small y, the y-component of the flow velocity can be ignored compared with the x-component and Eq. (1) can be simplified to:

$$v_g(x, t) = V_a - V_b \sin(kx - \omega t), \tag{2}$$

where $v_g(x, t)$ is the dimensional gas flow velocity at a time t at a location x. Following [12], our further analysis will be based on Eq. (2). This flow could describe a number of practically important configurations including pulsating vortex sheets and rings (e.g. [14,15]).

Ignoring the effects of the external (gravity) force, Basset (history) force, the Faxén correction to the viscous force, the shear induced and Magnus lift forces, the equation for particle dynamics can be presented as [16]:

$$\rho_p \vartheta \frac{\mathrm{d}v_p(x, t)}{\mathrm{d}t} = F^d + F^i + F^a, \tag{3}$$

where ρ_p and ϑ are the particle density and volume respectively, F^d, F^i and F^a are viscous drag, inertial and added-mass forces. F^i takes into account the effect of acceleration of the host gas on the particle, while F^a takes into account the effect of the accelerating particle on the host gas.

Eq. (3) is a simplified version of the general equation derived and discussed in [17].

The general expression for F^d can be presented as [18]:

$$F^d = \frac{1}{2} C_D \rho_g |v_g - v_p| (v_g - v_p) \pi R_p^2, \tag{4}$$

where ρ_g is gas density, C_D is the drag coefficient, depending on the particle Reynolds number

$$Re_p = \frac{2R_p\rho_g|v_g - v_p|}{\mu_g},$$

R_p is the particle radius, μ_g is the gas dynamic viscosity. In the Stokesian limit of small Re_p, $C_D = 24/Re_p$ and the expression for F^d is simplified to:

$$F^d = 6\pi R_p\mu_g(v_g - v_p). \tag{5}$$

Eq. (5) was derived in the limit $Re_p \ll 1$, but it can be used in practical applications for $Re_p \leqslant 0.5$ and even $Re_p \leqslant 2$ [18].

In the Stokesian limit the expressions for F^i and F^a for spherical particles were derived in the form [19–22,16]:

$$F^i = \rho_g\vartheta\frac{Dv_g}{Dt}, \tag{6}$$

$$F^a = \frac{1}{2}\rho_g\vartheta\left(\frac{Dv_g}{Dt} - \frac{\mathrm{d}v_p(x,t)}{\mathrm{d}t}\right), \tag{7}$$

where the substantial derivative is defined as:

$$\frac{Dv_g}{Dt} = \frac{\partial v_g}{\partial t} + v_g\frac{\partial v_g}{\partial x}.$$

Eqs. (6) and (7) were derived assuming that the particle size is much smaller than the characteristic length scale of the flow. This can be assumed valid in most of the practical applications mentioned above.

Restricting our analysis to the Stokesian approximation and remembering Eqs. (2), (3), (5), (6) and (7), the normalised equation for particle velocity can be presented as:

$$\frac{\mathrm{d}u_p}{\mathrm{d}\tau} = \frac{1}{\widetilde{St}}(u_g - u_p) + \frac{3\rho_g}{2\rho_0}u_b\cos(\tilde{x} - \tau)[1 - u_g], \tag{8}$$

where $u_g = v_g/V_\omega$, $u_p = v_p/V_\omega$, $\tau = \omega t$, $\tilde{x} = kx$,

$$\widetilde{St} = \frac{2\rho_0\omega R_p^2}{9\mu_g}, \quad \rho_0 = \rho_p + \frac{1}{2}\rho_g.$$

In most important practical applications, including medical aerosols, Diesel fuel sprays and Diesel particulate filters [6–8], $\rho_g \ll \rho_p$. This allows us to ignore the effects of inertial and added-mass forces, unless $\widetilde{St} \gg 1$, and simplify Eq. (8) to

$$\frac{\mathrm{d}u_p}{\mathrm{d}\tau} = \frac{1}{St}(u_g - u_p), \tag{9}$$

where

$$St = \frac{2\rho_p\omega R_p^2}{9\mu_g} \approx \widetilde{St}$$

is the Stokes number, v_g is given by Eq. (2). The generalisation of Eq. (9) to the case of non-Stokesian flow is discussed in Section 6. Until this section, the validity of the Stokesian approximation will be assumed. The interaction between particles and the effect of particles on gas are ignored.

The analysis of Eq. (9) is simplified considerably if it is re-written in the frame of reference moving with the phase velocity of the wave:

$$x_{\text{wave}} = x_{\text{stationary}} - V_\omega t. \tag{10}$$

The particle velocities in the wave and stationary frames of reference are linked by the following equation:

$$v_{p(\text{wave})} = v_{p(\text{stationary})} - V_\omega. \tag{11}$$

In view of Eqs. (9), (10) and (11), the particle trajectory in the frame of reference moving with the wave can be described by the following equation:

$$\frac{\mathrm{d}U_p}{\mathrm{d}\tau} = \frac{1}{St}(U_a - 1 - U_b \sin X - U_p), \tag{12}$$

where X is the distance in the moving frame of reference normalised by k^{-1}, U_p is the normalised particle velocity in the same frame of reference, $U_a = V_a/V_\omega$, $U_b = V_b/V_\omega$ (cf. the analysis of electron trajectories in plasma waves as discussed in [23]).

Eq. (12) can be rewritten in an alternative format:

$$\frac{\mathrm{d}^2X}{\mathrm{d}\tau^2} + \frac{1}{St}\frac{\mathrm{d}X}{\mathrm{d}\tau} - \frac{1}{St}(U_a - 1 - U_b \sin X) = 0. \tag{13}$$

If the contribution of the term

$$\frac{1}{St}\frac{\mathrm{d}X}{\mathrm{d}\tau}$$

in this equation could be ignored then its solution could be presented in terms of elliptical integrals [24]. This approximation is widely used for the analysis of charged particles/plasma wave interactions in collisionless plasma [23]. In the case of particle interaction with an oscillating flow, however, this approximation seems to be of limited practical use (viscous forces are the dominant). In the latter case another approximation of small St is expected to be important. As follows from the definition of St, the condition $St \ll 1$ is always satisfied for sufficiently small particles and/or small ω. Note that this condition should be viewed in connection with the corresponding condition for the Stokesian flow: $Re_p = 2\rho_g|v_g - v_p|R_p/\mu_g < 2$ [18].

Assuming that $St \ll 1$, Eq. (13) can be simplified to:

$$\frac{\mathrm{d}X}{\mathrm{d}\tau} - U_b(\beta - \sin X) = 0, \tag{14}$$

where, following [12], we introduced the new parameter $\beta = (U_a - 1)/U_b$.

Note that Eq. (14) is the exact equation for the Lagrangian trajectory of 'fluid particles' in the flow field given by Eq. (2). This means that in the zeroth approximation the relative motion of particles and fluid is not taken into account.

Considering the first approximation of the solution of Eq. (13) we assume that:

$$X = X_S + X_1, \tag{15}$$

where X_S is the solution of Eq. (14), $|X_1| \ll |X_S|$. Having substituted Eq. (15) into Eq. (13) and keeping only the linear terms with respect to X_1, we obtain the following equation for X_1:

$$\frac{\mathrm{d}X_1}{\mathrm{d}\tau} + a(\tau)X_1 = b(\tau), \tag{16}$$

where

$$a(\tau) = \cos X_s, \qquad b(\tau) = -St\frac{\mathrm{d}^2X_S}{\mathrm{d}\tau^2}.$$

Eq. (16) has a straightforward solution, satisfying the initial condition $X_1|_{t=0} = 0$:

$$X_1 = \frac{1}{\exp[\int_0^\tau a(\tau')\,\mathrm{d}\tau']}\int_0^\tau \left\{ b(\tau')\exp\left[\int_0^{\tau'} a(\tau'')\,\mathrm{d}\tau''\right]\right\}\mathrm{d}\tau'. \tag{17}$$

The form of this solution, however, seems to be rather complicated, without showing any new physics compared with the general numerical solution. The main focus of our further analysis will be on Eq. (14). The predictions of this equation will be compared with the numerical solution of Eq. (13) where appropriate.

3. Analytical solutions for small *St*

The format of the general solution of Eq. (14) depends on the value of β. If $|\beta| < 1$ then this solution can be presented as:

$$U_b(\tau - \tau_0) = \frac{1}{\sqrt{1-\beta^2}} \ln\left|\frac{\beta \tan\frac{X}{2} - \sqrt{1-\beta^2} - 1}{\beta \tan\frac{X}{2} + \sqrt{1-\beta^2} - 1}\right|\Bigg|_{X_0}^{X}, \tag{18}$$

where $X_0 = X(\tau_0)$.

For $|\beta| = 1$ this solution can be written as:

$$U_b(\tau - \tau_0) = \tan\left(\frac{\pi}{4} + \frac{\beta X}{2}\right) - \tan\left(\frac{\pi}{4} + \frac{\beta X_0}{2}\right). \tag{19}$$

For $|\beta| > 1$ this solution takes the form:

$$U_b(\tau - \tau_0) = \frac{2}{\sqrt{\beta^2-1}} \arctan\left[\frac{\beta \tan\frac{X}{2} - 1}{\sqrt{\beta^2-1}}\right]\Bigg|_{X_0}^{X}. \tag{20}$$

These solutions can be easily obtained using the substitution $u = \tan(X/2)$ [25].

In the limit $\beta \to 0$ (the mean flow velocity is equal to the wave phase velocity), Eq. (18) is simplified to:

$$U_b(\tau - \tau_0) = \ln\left|\tan\frac{X}{2}\right| - \ln\left|\tan\frac{X_0}{2}\right|. \tag{21}$$

The trajectories of the particles predicted by Eqs. (18)–(21) can be rather complicated. However, some important properties of these trajectories can be established even without the detailed analysis of the equations.

Let us assume that $-1 < \beta < 1$ and focus our analysis on Eq. (18). One can see that for $X = X_{\lim} \equiv \arcsin\beta$ and $\cos X_{\lim} > 0$:

$$\beta \tan\frac{X}{2} + \sqrt{1-\beta^2} - 1 = \beta\frac{1-\cos X_{\lim}}{\sin X_{\lim}} + \sqrt{1-\beta^2} - 1 = 0. \tag{22}$$

Thus, for $X \to X_{\lim}$ and $\cos X_{\lim} > 0$ the right-hand side of Eq. (18) becomes infinitely large and positive. This means that when X approaches $X_{\lim}$, the time τ is expected to become infinitely large, and both the first and the second derivative of X are expected to become infinitely small. This could happen only when the particles are grouped in the vicinity of $X = X_{\lim}$.

For the same range $-1 < \beta < 1$, $X = X_{\lim} \equiv \arcsin\beta$ and $\cos X_{\lim} < 0$:

$$\beta \tan\frac{X}{2} - \sqrt{1-\beta^2} - 1 = \beta\frac{1-\cos X_{\lim}}{\sin X_{\lim}} - \sqrt{1-\beta^2} - 1 = 0.$$

Thus, for $X \to X_{\lim}$ and $\cos X_{\lim} < 0$ the right-hand side of Eq. (18) approaches $-\infty$. This cannot satisfy Eq. (18) since the left-hand side of this equation is positive. Hence, the grouping can occur in the vicinity of $X = X_{\lim}$ only when $\cos X_{\lim} > 0$. It is interesting to mention that although this result was obtained for small Stokes numbers, it remains valid for finite *St*, provided that Eq. (9) remains valid (see Section 4), and even for non-Stokesian flows (see Section 6). The solution $X = \arcsin\beta$ satisfies Eq. (13) when both velocity and acceleration of particles are equal to zero regardless of the sign of $\cos X_{\lim}$. However, position $X = X_{\lim}$ can be reached only when $\cos X_{\lim} > 0$. An alternative proof of this statement is discussed in Section 4. Solution (21) for $\beta = 0$ can be considered as a limiting case of solution (18).

A similar property of the solution for $\beta = 1$ and $\beta = -1$ follows from Eq. (19) for $X \to X_{\lim} = (\pi/2) \pm 2\pi n$ and $X \to X_{\lim} = (-\pi/2) \pm 2\pi n$ respectively, where $n = 0, \pm 1, \pm 2, \ldots$. For $\beta = 1$: X can approach $X_{\lim}$ only from below ($X < X_{\lim}$) to ensure that the signs of the left and right-hand sides of Eq. (19) are the same. For the same reason, for $\beta = -1$: X can approach $X_{\lim}$ only from above $X > X_{\lim}$. Both results are consistent with the previous result obtained from Eq. (18), remembering that $\arcsin(\pm 1) = \pm(\pi/2) \pm 2\pi n$. In contrast to the solution for $-1 < \beta < 1$, in this case we have only one value of X over the 2π period which satisfies the equation $X = X_{\lim} = \arcsin\beta$, and $\cos X_{\lim} = 0$.

Solutions (18), (19) and (21) cannot be used when $X_0 = X_{\lim}$. However, as follows from Eqs. (12) and (13), in this case we can expect that the velocity and acceleration of particles are equal to zero and the particles will not move from their initial positions.

Now let us consider the case when $\beta > 1$. In the limit $\beta \to \infty$, Eq. (20) reduces to a trivial statement that

$$(U_a - 1)(\tau - \tau_0) = X - X_0. \tag{23}$$

Eq. (23) indicates that the particles are entrained by the flow (they move with the mean velocity of the flow). This is an expected result. β is large when the amplitude of flow oscillations is small, except in the trivial case when $U_a = 1$ (particles initially entrained by the flow do not change their positions relative to this flow). Hence the mean velocity of the flow dominates over the oscillations. For small Stokes numbers, the size of particles is expected to be small. Hence the contribution of the transitional period, before the particles are fully entrained by the flow, can be ignored.

It can be shown (see Appendix A) that Eq. (20) predicts the following particle average velocity:

$$\overline{U_p} = \frac{\Delta X}{\Delta \tau} = U_b\sqrt{\beta^2 - 1} = (U_a - 1)\sqrt{1 - \frac{1}{\beta^2}}. \tag{24}$$

In the limit when $\beta \to \infty$, $\overline{U_p} = (U_a - 1)$ as expected.

Eq. (24) shows that the oscillations of the flow produce an additional effective drag on the particle velocity. In the presence of oscillations, $\overline{U_p}$ is always smaller than in the absence of oscillations. In the limit $|\beta| \to 1$, $\overline{U_p} \to 0$ and the grouping phenomenon can be expected, in agreement with Eq. (19).

In the next section, the focus will be on Eq. (13) which will be analysed for $|\beta| \leqslant 1$ in the vicinity of the points where $X = X_{\lim}$.

4. Converging and repelling trajectories

As already mentioned in Section 3, for $X = X_{\lim} \equiv \arcsin\beta$, Eq. (13) is satisfied for

$$\frac{\mathrm{d}^2 X}{\mathrm{d}\tau^2} = 0 \quad \text{and} \quad \frac{1}{St}\frac{\mathrm{d}X}{\mathrm{d}\tau} = 0.$$

These conditions mean that the particle position in the frame of reference moving with the wave phase velocity does not change. In other words, once the particles have reached this position their further movement in this frame of reference stops. If a number of particles reaches this position they become grouped, using the terminology introduced by [12]. Since equation $X = \arcsin\beta$ has a real solution only when $|\beta| \leqslant 1$, we can expect that grouping is possible only if the latter inequality is satisfied.

The points satisfying equation $X = X_{\lim} = \arcsin\beta$ are expected to be grouping points only when particle trajectories in the vicinity of these points converge to $X_{\lim}$ when $\tau \to \infty$ (i.e. particle trajectories are converging). In the opposite case, when the distance between X and $X_{\lim}$ increases when $\tau \to \infty$ (i.e. particle trajectories are repelling), no grouping is expected to take place in the vicinity of $X_{\lim}$. To establish the type of trajectory expected in the vicinity of $X_{\lim}$ let us assume that

$$X = X_{\lim} + X_1, \tag{25}$$

where $|X_1| \ll X_{\lim}$ and $|X_1| \ll 1$.

Having substituted Eq. (25) into Eq. (13) we obtain, remembering the definition of $X_{\lim}$ and the condition $|X_1| \ll 1$:

$$\frac{\mathrm{d}^2 X_1}{\mathrm{d}\tau^2} + \frac{1}{St}\frac{\mathrm{d}X_1}{\mathrm{d}\tau} + \frac{U_b \cos X_{\lim}}{St} X_1 = 0. \tag{26}$$

The general solution of Eq. (26) can be presented as:

$$X_1 = X_{101}\exp(\alpha_1\tau) + X_{102}\exp(\alpha_2\tau), \tag{27}$$

where

$$\alpha_{1,2} = \frac{1}{2St}\left[-1 \pm \sqrt{1 - 4U_b St\cos X_{\lim}}\right], \tag{28}$$

coefficients X_{101} and X_{102} are determined from the initial conditions for X_1 and its first derivative.

As one can see from Eqs. (27) and (28), for $\cos X_{\lim} > 0$, $X_1 \to 0$ when $\tau \to \infty$, regardless of the values of X_{101} and X_{102} and other parameters.

If $0 < 4U_bSt\cos X_{\rm lim} < 1$ then for sufficiently large times the contribution of the second term in Eq. (27) can be ignored compared with the contribution of the first term in this equation unless $X_{101} = 0$. In this case, an order of magnitude of the characteristic time during which the grouping is expected to take place can be estimated as:

$$\tau_{\rm group} = \frac{2St}{1-\sqrt{1-4U_bSt\cos X_{\rm lim}}}. \tag{29}$$

For sufficiently small St, Eq. (29) can be simplified to:

$$\tau_{\rm group} = \frac{1}{4U_b\cos X_{\rm lim}}. \tag{30}$$

As follows from Eqs. (29) and (30), $\tau_{\rm group} \to \infty$ when $U_b\cos X_{\rm lim} \to 0$. This means that even in the case when the condition $|\beta| < 1$ for grouping is satisfied, the grouping cannot actually take place for any finite interval of time. The second necessary condition for grouping in this case can be presented as:

$$\frac{2St}{1-\sqrt{1-4U_bSt\cos X_{\rm lim}}} < \tau_{\rm lim}, \tag{31}$$

where $\tau_{\rm lim}$ is the characteristic time scale of the process. This parameter is determined by the underlying physics of the process (e.g. the characteristic time of spray penetration (see [26,27]).

If $4U_bSt\cos X_{\rm lim} > 1$ then Eq. (27) can be simplified to:

$$X_1 = \exp\left[-\frac{\tau}{2St}\right]\left\{X_{101}\exp(\omega_{\rm lim}\tau{\rm i}) + X_{102}\exp(-\omega_{\rm lim}\tau{\rm i})\right\}, \tag{32}$$

where

$$\omega_{\rm lim} = \frac{1}{2St}\sqrt{4U_bSt\cos X_{\rm lim} - 1},$$

is the frequency of oscillations of the particle trajectories near $X = X_{\rm lim}$, ${\rm i} = \sqrt{-1}$.

Note that coefficients X_{101} and X_{102} in Eq. (32) are allowed to be complex:

$$\left.\begin{aligned} X_{101} &= X_{101R} + {\rm i}X_{101I} \\ X_{102} &= X_{102R} + {\rm i}X_{102I} \end{aligned}\right\}.$$

Since the left-hand side of Eq. (32) is real, this equation can be simplified to:

$$X_1 = \exp\left[-\frac{\tau}{2St}\right]\left\{X_{\omega1}\cos(\omega_{\rm lim}\tau) + X_{\omega2}\sin(\omega_{\rm lim}\tau)\right\}, \tag{33}$$

where the new constants $X_{\omega1}$ and $X_{\omega2}$ are defined as:

$$\left.\begin{aligned} X_{\omega1} &= X_{101R} + X_{102R} \\ X_{\omega2} &= -X_{101I} + X_{102I} \end{aligned}\right\}.$$

In this case, an order of magnitude of the characteristic time during which the grouping is expected to take place can be estimated as:

$$\tau_{\rm group} = 2St. \tag{34}$$

Eq. (34) shows that at small St, the time delay required for grouping to take place can be rather short.

If $\cos X_{\rm lim} < 0$, $X_1 \to \infty$ when $\tau \to \infty$, except when $X_{102} = 0$. This is an unstable solution and no grouping is expected in this case.

If $\cos X_{\rm lim} = 0$ then Eq. (27) is simplified to:

$$X_1 = X_{101}\exp\left[-\frac{\tau}{St}\right] + X_{102}. \tag{35}$$

Since the values of X_{102} for different particles can be different, no grouping is expected to take place in the general case.

The dependence of the types of various particle trajectories on the values of $4U_bSt$ and $X_{\rm lim}$ is schematically shown in Fig. 1 in the form of a γ–$X_{\rm lim}$ diagram, where $\gamma = (4U_bSt)^{-1}$. Zone 1 refers to converging trajectories without oscillations. Zone 2 refers to converging trajectories with oscillations. Zone 3 refers to repelling trajectories.

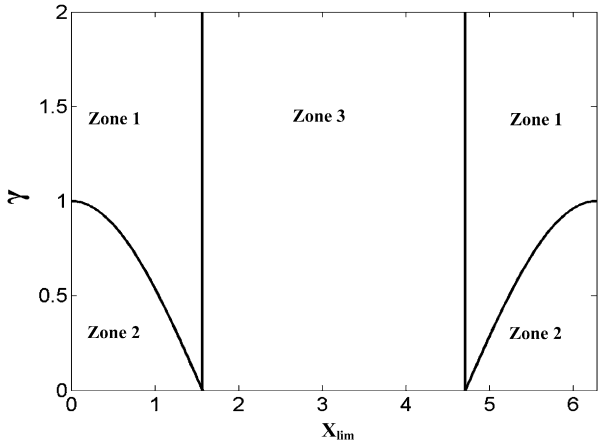

Fig. 1. Schematic presentation of Zones 1, 2 and 3 on the γ–$X_{\rm lim}$ diagram, where $\gamma = (4U_b St)^{-1}$. Zone 1 refers to converging trajectories without oscillations. Zone 2 refers to converging trajectories with oscillations. Zone 3 refers to repelling trajectories.

5. Analytical versus numerical results

In this section the trajectories of particles are analysed based on the numerical solution of Eq. (13) and the analytical solutions (18)–(20) and (27) for the values of parameters realistic for sprays in Diesel engines [28]. For the numerical solution, the higher order single point method – the fourth order Runge–Kutta method – was used [29]. We took ω and k equal to 10^5 rad/s and 2000 rad/m respectively. These values of ω and k give a wave phase velocity equal to 50 m/s. In what follows this comparison is performed separately for the case of small Stokes numbers and the trajectories in the vicinity of $X = X_{\rm lim}$ for finite Stokes numbers.

5.1. Particle trajectories for small Stokes numbers

Taking $V_a = 60$ m/s and $V_b = 20$ m/s, we obtain: $U_a = 1.2$, $U_b = 0.4$ and $\beta = 0.5$. This allows us to use the solution of Eq. (14) in the form (18). The analysis was performed for the following values of Stokes number: 0.1, 0.4 and 0.9. For realistic Diesel engine conditions this corresponds to particle (droplet) radii R_p equal to 0.5 μm, 1 μm and 1.5 μm respectively, if we take the dynamic viscosity of the ambient gas equal to 3.3×10^{-5} Ns/m^2 and particle (droplet) density equal to 600 kg/m^3. Ambient gas density is taken equal to 15.7 kg/m^3. For these values of parameters, Eq. (9) is valid with comfortable margins.

We consider two values of X at $\tau = 0$ (initial conditions): $X_0 = 0$ and $X_0 = 2$. These illustrate two starting points over the period 2π. In all cases the values of velocity are chosen so that the initial accelerations of droplets are equal to zero. This is achieved when:

$$\frac{{\rm d}X}{{\rm d}\tau} = U_a - 1 - U_b \sin X_0. \tag{36}$$

For the chosen values of U_a and U_b this condition can be rewritten as:

$$\frac{{\rm d}X}{{\rm d}\tau} = 0.2 - 0.4 \sin X_0.$$

The plots of X versus τ for these initial conditions are shown in Fig. 2. Solid curves refer to the analytical solution based on Eq. (18). Dashed and dashed-dotted curves refer to the results of numerical calculations based on Eq. (13) with $St = 0.4$ and $St = 0.9$ respectively. The curves obtained from numerical calculations based on Eq. (13) and $St = 0.1$ coincide with those obtained based on the analytical solution (Eq. (18)). The values of X_0 are indicated near the curves. As follows from this figure, the analytical and numerical results are very close even in the case when the condition $St \ll 1$, based on which the analytical solution was obtained, is not satisfied. For all X_0 both analytical and numerical solutions converge to $X_{\rm lim} = \arcsin \beta = \arcsin 0.5 = \pi/6 \approx 0.52$, in agreement with the result predicted in Section 3.

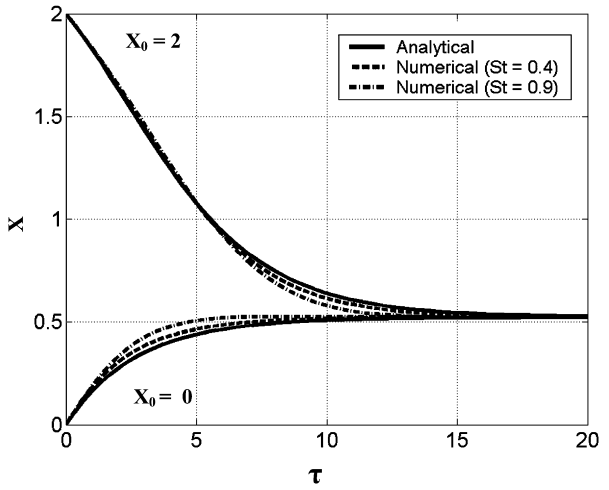

Fig. 2. The plots of X versus τ for $V_a = 60$ m/s, $V_b = 20$ m/s, $V_w = 50$ m/s ($\beta = 0.5$) and two values of X_0: 0 and 2. Solid curves refer to the analytical results obtained based on Eq. (18). Dashed and dashed-dotted curves refer to the results of numerical calculations based on Eq. (13) and $St = 0.4$ and $St = 0.9$ respectively. The curves obtained from numerical calculations based on Eq. (13) and $St = 0.1$ coincide with those obtained using the analytical solution (Eq. (18)). The values of X_0 are indicated near the curves.

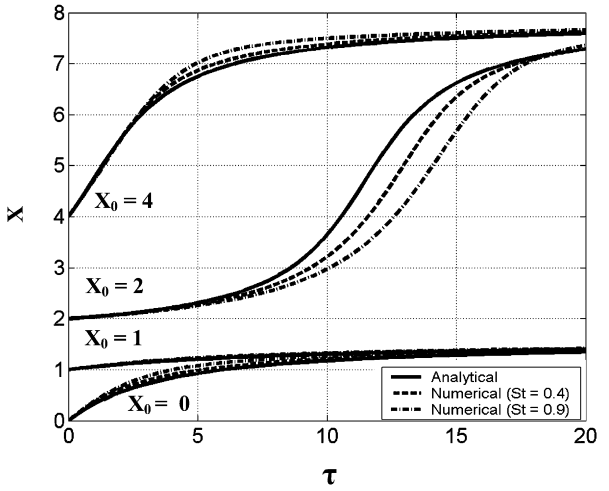

Fig. 3. The same as Fig. 2 but for $V_a = 70$ m/s ($\beta = 1$). Four values of X_0 are considered: 0, 1, 2 and 4 (indicated near the curves).

The plots similar to those shown in Fig. 2 but for $U_a = 1.4$ and $X_0 = 0$, 1, 2, 4 are shown in Fig. 3. In this case $\beta = 1$ and the comparison between the results of numerical analysis of Eq. (13) and the analytical solution (19) has been performed for the same St as in Fig. 2. As one can see from Fig. 3, for $X_0 = 0$ the predictions of numerical and analytical solutions are very close, even in the case when the condition $St \ll 1$ is not satisfied. Both these solutions predict that $X \to \pi/2 \approx 1.571$ when $\tau \to \infty$, in agreement with Eq. (19) (see the discussion in Section 3). For $X_0 = 2$ the predictions of numerical and analytical solutions appear to be noticeably different for $8 < \tau < 18$. However, even in this case the qualitative behaviours of the curves predicted by these solutions are similar. Both solutions predict that $X \to \pi/2 + 2\pi \approx 7.854$ when $\tau \to \infty$. The plots for $X_0 = 0$ and $X_0 = 1$ converge to $X \to \pi/2 \approx 1.571$ when $\tau \to \infty$, while the plots for $X_0 = 2$ and $X_0 = 4$ converge to $X \to \pi/2 + 2\pi \approx 7.854$ when $\tau \to \infty$. This agrees with the results of qualitative analysis of Eq. (19) presented in Section 3: X can approach $X_{\lim}$ from one side only (from below in our case) to ensure that the sign of the right-hand side of this equation remains positive.

The results of the analysis, similar to the one shown in Figs. 2 and 3 but for $U_a = 1.2$ and $U_b = 0.1$, $St = 0.9$ and $X_0 = 0$,2, are shown in Fig. 4. In this case $\beta = 2$. As follows from Fig. 4, the analytical and numerical results are very close. In contrast to Figs. 2 and 3, no limiting values for X at $\tau \to \infty$ can be seen for both X_0. The values of X oscillate around the inclined line. The tangent of this line shows the average droplet velocity $\overline{U_p}$, and its value appears to be close to the one predicted by Eq. (24): $\overline{U_p} = (U_a - 1)\sqrt{1 - 1/\beta^2} = 0.2 \times 0.866 \approx 0.173$.

5.2. Particle trajectories in the vicinity of $X = X_{\lim}$

Let us consider the same values of parameters as used in Fig. 2, except that we take $St = 40.4$. This corresponds to $R_p = 10$ μm (a more realistic value of this parameter when compared with the values used in Figs. 2–4). For the chosen values of velocities and densities the second term on the right-hand side of Eq. (8) can be non-negligible compared with the first term in the right-hand side of the same equation. Hence, the results of the analysis for this St will illustrate the qualitative tendency of the processes rather than quantitative characteristics. A comparison of the particle trajectories predicted by the numerical solution of Eq. (13) and the analytical solution (27) is performed. This comparison is meaningful only in the case when X is close to $X_{\lim}$.

For the chosen values of velocities, $\beta = 0.5$. This gives us an infinite number of points where $X = X_{\lim}$. Firstly, our analysis is focused on $X_{\lim} = \pi/6 = 0.5236$. In this case $\cos X_{\lim} > 0$ and we expect to have a converging trajectory.

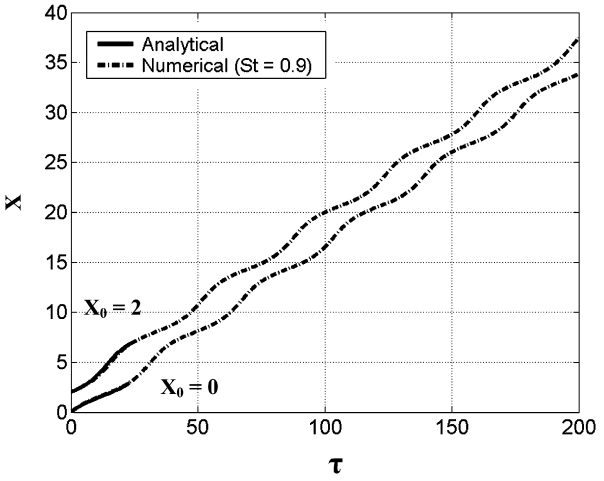

Fig. 4. The same as Figs. 2 and 3 but for $V_a = 60$ m/s and $V_b = 5$ m/s ($\beta = 2$). The curves obtained from numerical calculations based on Eq. (13) and $St = 0.4$ are not shown in the figure. They are very close to those obtained using the analytical solution (Eq. (18)). Two values of X_0 are considered: 0 and 2 (indicated near the curves).

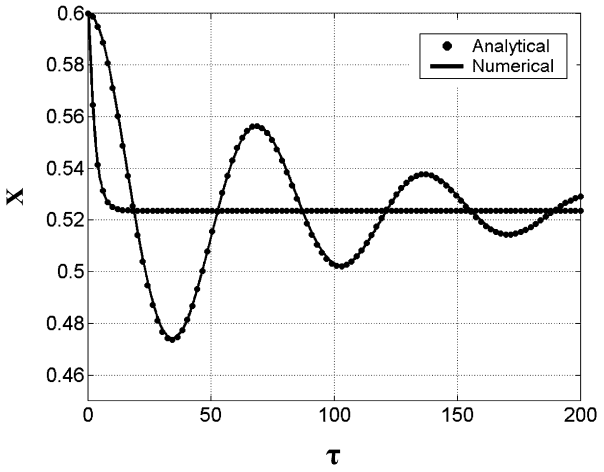

Fig. 5. The plots describing damped oscillations refer to X versus τ for $V_a = 60$ m/s, $V_b = 20$ m/s, $V_w = 50$ m/s ($\beta = 0.5$) ($St = 40.4$) and $X_0 = 0.6$. The plots describing monotonically decreasing X refer to the same values of parameters as above but for $St = 0.4$. The solid curves refer to the results of numerical solution of Eq. (13), while filled circles refer to the results predicted by Eq. (33).

Let us take the initial value of $X = X_0 = 0.6$. In this case the initial deviation of X from $X_{\lim}$ is $X_{10} = X_0 - X_{\lim} = 0.0764 \ll 1$ and we expect that Solution (27) is applicable. The second initial condition is taken for the first derivative of X:

$$\left.\frac{\mathrm{d}X}{\mathrm{d}\tau}\right|_{\tau=0} = U_{\mathrm{in}}.$$

Using the above mentioned values of parameters we obtain:

$$4U_b St \cos X_{\lim} = 55.98 > 1.$$

This means that we can expect an oscillatory converging trajectory described by Eq. (33) with

$$\omega_{\lim} = \frac{7.415}{2 \times 40.4} = 0.092.$$

Remembering the above described initial conditions we arrive at the following system of equations to determine the unknown coefficients $X_{\omega 1}$ and $X_{\omega 2}$:

$$\left.\begin{array}{l} X_{\omega 1} = 0.0764 \\ \frac{\mathrm{d}X}{\mathrm{d}\tau} = \frac{\mathrm{d}X_1}{\mathrm{d}\tau} = -\frac{1}{2St} X_{\omega 1} + \omega_{\lim} X_{\omega 2} = U_{\mathrm{in}} \end{array}\right\}. \tag{37}$$

Rearranging the second equation we obtain:

$$X_{\omega 2} = \frac{1}{2\omega_{\lim} St} X_{\omega 1} + \frac{U_{\mathrm{in}}}{\omega_{\lim}}.$$

In the case when $U_{\mathrm{in}} = 0$: $X_{\omega 2} = 0.01$.

The plots of X versus τ, as calculated based on Eqs. (13) and (33) for the above mentioned values of parameters, are shown in Fig. 5 (oscillating X). The solid curve refers to the results of numerical solution of Eq. (13), while filled circles refer to the results predicted by Eq. (33). As one can see from this figure, the numerical and analytical results practically coincide. Both these results predict damped oscillations and slow convergence of X to $X_{\lim} = \pi/6 \approx 0.52$. This agrees with the results of the analysis presented in Section 4 (see Zone 2 in Fig. 1). The characteristic grouping time, as estimated from Eq. (34), gives: $\tau_{\mathrm{group}} \approx 81$. The order of magnitude of this time agrees with the one which can be obtained from Fig. 5.

At the next stage we consider the same parameter values as above, but take $St = 0.4$. This corresponds to $R_p = 1$ μm. In this case, $4U_b St \cos X_{\lim} = 0.55426$ and the general solution of Eq. (26) can be presented in the form (27)

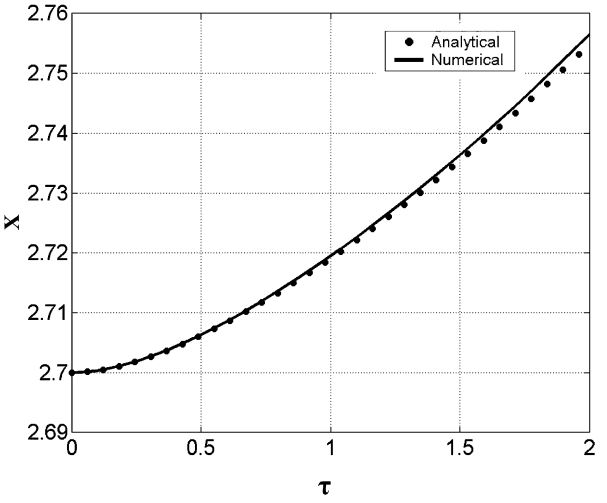

Fig. 6. The same as Fig. 5 for $St = 40.4$ but for $X_0 = 2.7$ in the range $0 \leqslant \tau \leqslant 2$.

with $\alpha_1 = -0.4155$ and $\alpha_2 = -2.0845$. Taking the same initial conditions as in the previous example, we arrive at the following system of equations to determine the unknown coefficients X_{101} and X_{102} in Eq. (27):

$$\left.\begin{array}{l} X_{101} + X_{102} = 0.0764 \\ \alpha_1 X_{101} + \alpha_2 X_{102} = U_{\text{in}} \end{array}\right\}. \tag{38}$$

The solution of this system can be presented as:

$$\left.\begin{array}{l} X_{101} = \frac{0.0764\alpha_2 - U_{\text{in}}}{\alpha_2 - \alpha_1} \\ X_{102} = \frac{0.0764\alpha_1 - U_{\text{in}}}{\alpha_1 - \alpha_2} \end{array}\right\}. \tag{39}$$

In the case when $U_{\text{in}} = 0$, $X_{101} = 0.095$ and $X_{102} = -0.019$.

The plots of X versus τ, as calculated based on Eqs. (13) and (27) for the above mentioned values of parameters, are also shown in Fig. 5 (monotonically decreasing X). The solid curve refers to the results of numerical solution of Eq. (13), while filled circles refer to the results predicted by Eq. (27). As one can see from this figure, the numerical and analytical results practically coincide, as in the previous case. Both these results predict monotonic convergence of X to the same X_{lim} as in the previous case. This agrees with the results of the analysis presented in Section 4 (see Zone 1 in Fig. 1). The characteristic grouping time, as estimated from Eq. (29), gives $\tau_{\text{group}} \approx 2.4$. The order of magnitude of this time agrees with the one which can be obtained from Fig. 5.

Next we consider the same parameters as used in Fig. 5 for $St = 0.4$ except we take $X_{\text{lim}} = 5\pi/6 = 2.618$ and $X_0 = 2.7$. In this case $\cos X_{\text{lim}} < 0$ and we expect to have a repelling trajectory. The initial deviation of X from X_{lim} is $X_{10} = X_0 - X_{\text{lim}} = 0.082 \ll 1$ and we expect that solution (27) is applicable. The second initial condition for the first derivative of X is taken in the form (36) as in the cases analysed in Section 5.1. Remembering that in this case St$= 0.4$, we obtain $4U_b St \cos X_{\text{lim}} = -0.55426$ and the general solution of Eq. (26) can be presented in the form (27) with $\alpha_1 = 0.308$ and $\alpha_2 = -2.809$. In this case Solution (39) can be rewritten as:

$$\left.\begin{array}{l} X_{101} = \frac{0.082\alpha_2 - U_{\text{in}}}{\alpha_2 - \alpha_1} \\ X_{102} = \frac{0.082\alpha_1 - U_{\text{in}}}{\alpha_1 - \alpha_2} \end{array}\right\}. \tag{40}$$

In the case when $U_{\text{in}} = 0$, $X_{101} = 0.074$ and $X_{102} = 0.008$.

The plots X versus τ, as calculated based on Eqs. (13) and (27) for the above mentioned values of parameters, including α_1 and α_2, are shown in Fig. 6. The solid curve refers to the results of numerical solution of Eq. (13), while filled circles refer to the results predicted by Eq. (27). As one can see from this figure, the numerical and analytical results practically coincide, as in the case shown in Fig. 5. Both these results predict monotonic divergent trajectories. This agrees with the results of the analysis presented in Section 4 (see Zone 3 in Fig. 1). Note that for larger τ

the trajectories predicted by the numerical solution eventually converge to a certain $X_{\lim}$, but this effect cannot be predicted by the simple solutions described in Section 4.

6. Non-Stokesian trajectories

In the following analysis it will be assumed that the inertial and added-mass forces can be ignored not only for the Stokesian trajectories, but also in the general case of non-Stokesian trajectories. In this case, Eq. (13) can be applied for the analysis of non-Stokesian trajectories if Stokes number St is replaced by the equivalent Stokes number $St_{\rm eq}$ defined as:

$$St_{\rm eq} = \frac{8\rho_p \omega R_p}{3C_D \rho_g |v_g - v_p|}, \tag{41}$$

where the drag coefficient C_D is estimated as [30] $C_D = 24/Re_p$ when $Re_p \leqslant 2$ (Stokesian flow),

$$C_D = \frac{24}{Re_p}\left[1 + 0.15 Re_p^{0.687}\right]$$

when $2 < Re_p < 500$ (Allen flow), and $C_D = 0.44$ when $Re_p \geqslant 500$ (Newton flow). In the case when $Re_p \leqslant 2$, $St_{\rm eq} = St$.

Remembering the definition of $St_{\rm eq}$ we can see that in the case of non-Stokesian flow, $St_{\rm eq}$ is a complicated function of droplet velocity. This makes Eq. (13) strongly non-linear. Let us rewrite Eq. (13) for non-Stokesian trajectories in the form of the system of equations:

$$\left.\begin{aligned} \dot{X} &= Y \equiv P(X, Y) \\ \dot{Y} &= \tfrac{-Y + a - b\sin X}{St_{\rm eq}(Y)} \equiv Q(X, Y) \end{aligned}\right\}, \tag{42}$$

where $Y \equiv U_p$ is the dimensionless droplet velocity in the wave frame of reference, it is explicitly indicated that $St_{\rm eq}$ is a function of Y (see Eq. (41)), $a = U_a - 1$, $b = U_b$. Without loss of generality we assume that a, b and $St_{\rm eq}$ are positive. System (42) can be analysed using the conventional technique described in a number of well known textbooks (e.g. [31,32]). The details are given in Appendix B. The general analysis of Eq. (13) with St replaced by $St_{\rm eq}$ is possible only using numerical methods. Some results of the numerical analysis of this equation are presented below.

As in the case of Section 5, for the numerical solution of Eq. (13) with $St = St_{\rm eq}$ defined by Eq. (41), the fourth order Runge–Kutta method was used [29]. The plots of X versus τ for $V_a = 60$ m/s, $V_b = 20$ m/s, $V_w = 50$ m/s ($\beta = 0.5$) and $R_p = 10$ μm are presented in Fig. 7 (solid curves). ω and k are taken equal to 10^5 rad/s and 2000 rad/m respectively. The dynamic viscosity of the ambient gas, gas and particle densities are the same as in Section 5. Six values of the initial particle positions X_0 were considered: 0, 1, 2, 3, 4 and 5.

As one can see from this figure, the trajectories for $X_0 = 0$, 1 and 2 converge to $X_{\lim} = 0.52$, while the trajectories for $X_0 = 3$, 4 and 5 converge to $X_{\lim} = 6.80$. For both values of $X_{\lim}$, $\cos X_{\lim} > 0$. The fact that particle trajectories converge at these values of $X_{\lim}$ was predicted by our simplified analysis of Stokesian trajectories for small St (cf. Fig. 2) and by a more general analytical approach discussed in Appendix B. In contrast to the case shown in Fig. 2, the trajectories in Fig. 7 (solid curves) approach to $X_{\lim}$ not monotonically, but with oscillations. These oscillations have some similarities with the ones shown in Fig. 5 for fixed St. In the general case, these equilibria are expected to be foci, as discussed in Appendix B.

In Fig. 8 the same trajectories as in Fig. 7 are shown but in the (X–U_p) plane. The initial moments of time $\tau = 0$ (when $X(\tau = 0) = X_0$) and time $\tau = 10$ for the relevant trajectories are indicated on the figure. Numbers near the points corresponding to $\tau = 10$ show the values of X_0 of the trajectories. As in the case of Fig. 7, the oscillatory convergence of trajectories to $X_{\lim}$ can be clearly seen. Note that at the convergence points, where grouping takes place, $U_p = 0$. The fact that both equilibrium points are foci is more clearly seen in this figure than in Fig. 7.

The plots Re_p versus τ for $X_0 = 0$ and 2 are shown in Fig. 9(a) for the same parameters as in Figs. 7–8. As can be seen in Fig. 9(a), in most cases Re_p is well above 2, and the flow is expected to be non-Stokesian. For large τ, $Re_p \to 0$. This is expected for the points where grouping takes place.

The dashed plots of X versus τ shown in Fig. 7 refer to the same parameters as the solid plots, but for ω and k equal to 10^2 rad/s and 20 rad/m respectively. In this case, the value of wave phase velocity is expected to be the same as

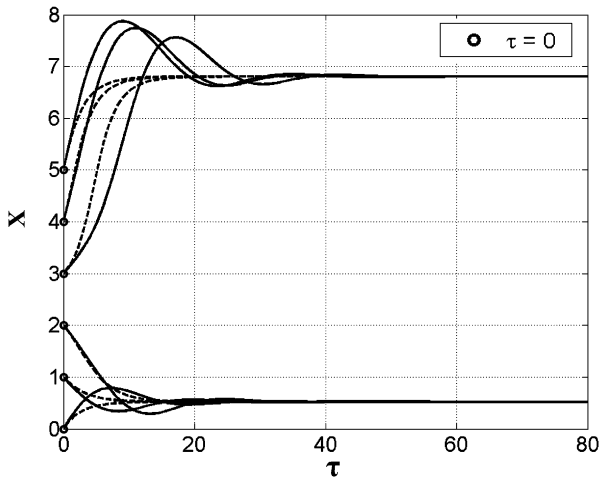

Fig. 7. The solid plots refer to X versus τ for $V_a = 60$ m/s, $V_b = 20$ m/s, $V_w = 50$ m/s ($\beta = 0.5$), $R_p = 10$ μm. ω and k are taken equal to 10^5 rad/s and 2000 rad/m respectively. The dynamic viscosity of the ambient gas is assumed to be equal to 3.3×10^{-5} Ns/m^2. Gas and particle densities are taken equal to 15.7 kg/m^3 and 600 kg/m^3 respectively. The dashed plots refer to the same parameters as above except ω and k are taken equal to 10^3 rad/s and 20 rad/m respectively.

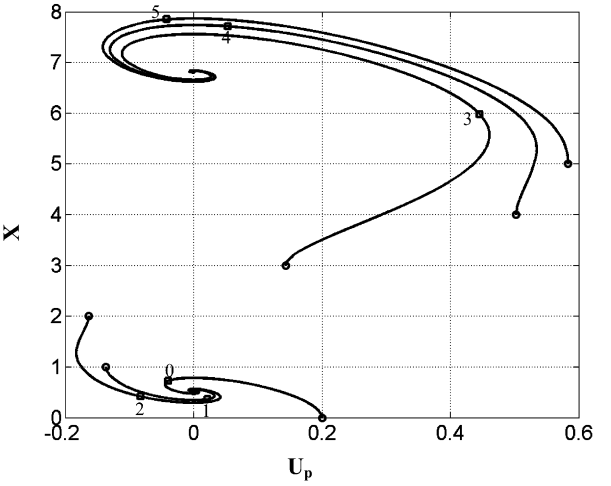

Fig. 8. The same as Fig. 7 (solid plots) but in the U_p–X plane. The initial values of X_0 are indicated near the plots alongside with the sequential moments of time.

before, but the value of St_{eq} is expected to be about 2 orders of magnitude less. As in the previous case, the trajectories for $X_0 = 0$, 1 and 2 converge to $X_{\text{lim}} = 0.52$, while the trajectories for $X_0 = 3$, 4 and 5 converge to $X_{\text{lim}} = 6.80$. In contrast to the previous case, however, the new trajectories in Fig. 13 approach to X_{lim} not with oscillations, but monotonically (cf. Fig. 5 for fixed St). The difference between the trajectories shown in Fig. 7 is related to the above-mentioned difference in the values of St_{eq}. As in the case of fixed St, the character of approach of particle trajectories to X_{lim} depends on St_{eq}. If St_{eq} is so small that $4U_b St_{\text{eq}} \cos X_{\text{lim}} < 1$ one would expect monotonic trajectories. In the opposite case when $4U_b St_{\text{eq}} \cos X_{\text{lim}} > 1$ the trajectories are expected to be oscillatory. In Section 4 this was proven for the case of fixed St and X close to X_{lim}. In the general case these equilibrium points correspond to stable nodes (see Appendix B).

In Fig. 10 the same trajectories as in Fig. 7 (dashed curves) are shown but in the (X–U_p) plane. The initial moments of time $\tau = 0$ (when $X(\tau = 0) = X_0$) and time $\tau = 10$ for the relevant trajectories are indicated on the figure. Numbers near the points corresponding to $\tau = 10$ show the values of X_0 of the trajectories. As can be seen from this figure, the trajectories corresponding to $X_0 = 0$, 1, 4 and 5 practically reach the grouping points at $\tau = 10$, in agreement with Fig. 7 (dashed plots). As in the case of Fig. 7 (dashed plots), the monotonic convergence of trajectories along the X-axis to X_{lim} can be clearly seen. Note that at the convergence points, where grouping takes place, $U_p = 0$, as in the case shown in Fig. 8. The fact that the equilibrium points are stable nodes is more clearly seen in this figure than in Fig. 7 (dashed plots).

The plots Re_p versus τ for $X_0 = 0$ and 2 are shown in Fig. 9(b) for the same parameters as in Figs. 7 (dashed curves) and 10. As can be seen in Fig. 9(b), in most cases Re_p is well above 2, and the flow is expected to be non-Stokesian. For large τ, $Re_p \to 0$, as in the case shown in Fig. 9(a).

The plots of X versus τ for the same parameters as in Fig. 7 (solid curves), except for $V_a = 60$ m/s and $V_b = 10$ m/s, are shown in Fig. 11. In this case we have $\beta = 1$. For $X_0 = 0$ and 1 the trajectories are rather similar to those shown in Fig. 3. These trajectories approach corresponding values of X_{lim} from below as predicted in Section 3 for the case of small fixed values of St. However, for trajectories corresponding to $X_0 = 2$, 3, 4 and 5 we can observe a new phenomenon when grouping at $X_{\text{lim}} = (\pi/2) + 2\pi \approx 7.85$ is unstable and the trajectory jumps to the next grouping level $X_{\text{lim}} = (\pi/2) + 4\pi \approx 14.14$. The likelihood of unstable equilibria in the vicinity of these equilibrium points is discussed in Appendix B.

In Fig. 12 the same trajectories as in Fig. 11 are shown but in the (X–U_p) plane. The initial moments of time $\tau = 0$ (when $X(\tau = 0) = X_0$) and time $\tau = 10$ for the relevant trajectories are indicated, as in Figs. 8 and 10. Numbers near

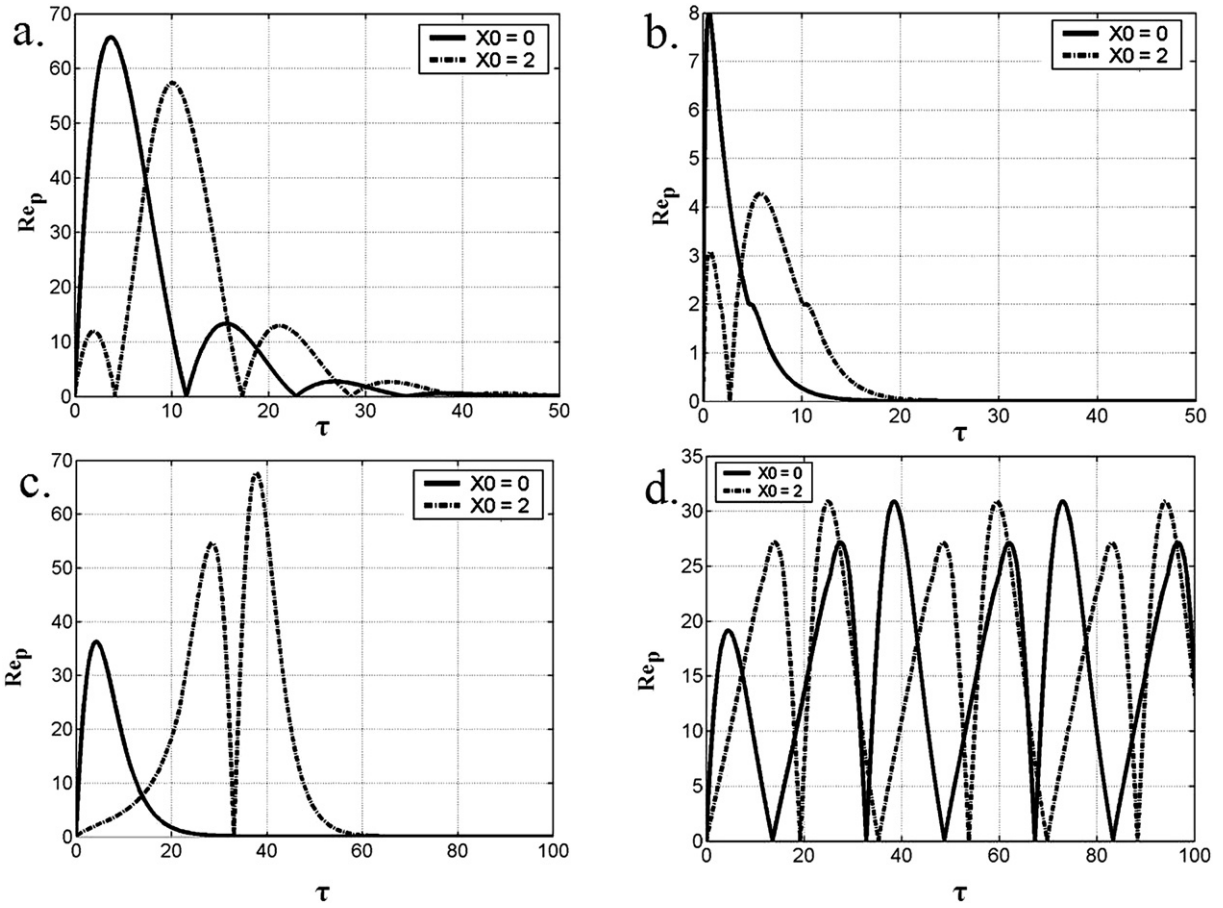

Fig. 9. The plots of Re_p versus τ for the same parameters as in Figs. 7 (solid plots) and 8 with $X_0 = 0$ and 2 (a). The plots of Re_p versus τ for the same parameters as in Figs. 7 (dashed plots) and 10 with $X_0 = 0$ and 2 (b). The plots of Re_p versus τ for the same parameters as in Figs. 11 and 12 with $X_0 = 0$ and 2 (c). The plots of Re_p versus τ for the same parameters as in Figs. 13 and 14 with $X_0 = 0$ and 2 (d).

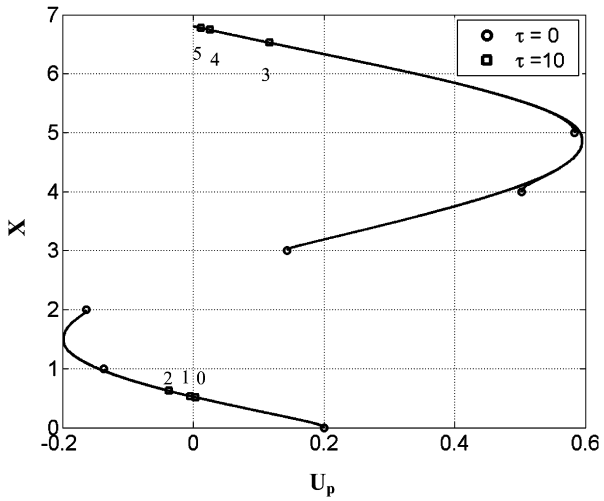

Fig. 10. The same as Fig. 7 (dashed plots) but in the U_p–X plane. The initial values of X_0 are indicated near the plots alongside with the sequential moments of time.

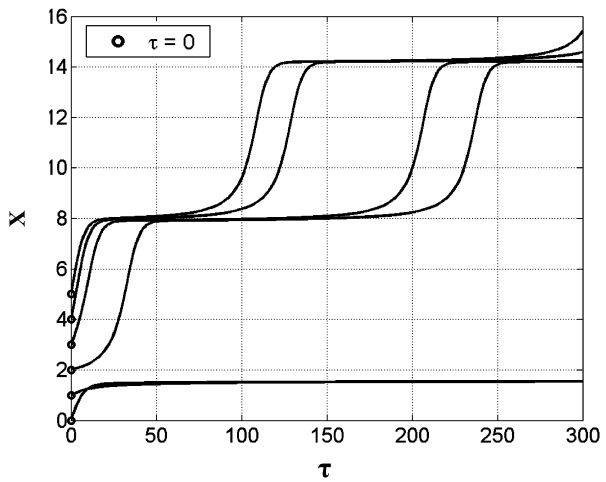

Fig. 11. The plots of X versus τ for the same parameters as in Fig. 7 (solid plots) except for $V_a = 60$ m/s and $V_b = 10$ m/s ($\beta = 1$).

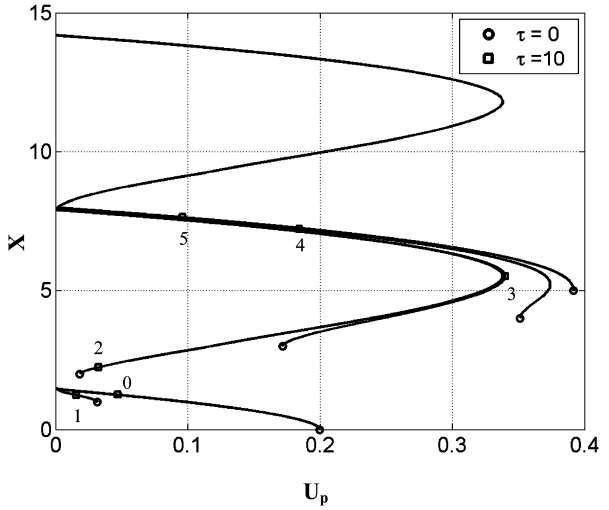

Fig. 12. The same as Fig. 11 but in the U_p–X plane. The initial values of X_0 are indicated near the plots alongside with the sequential moments of time.

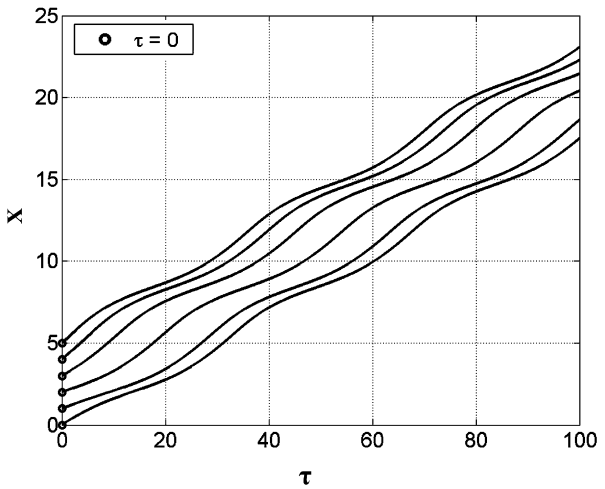

Fig. 13. The plots of X versus τ for the same parameters as in Fig. 7 (solid plots) except for $V_a = 60$ m/s and $V_b = 5$ m/s ($\beta = 2$).

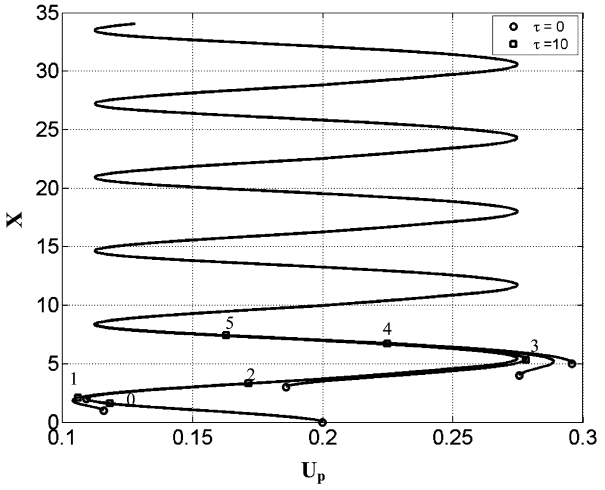

Fig. 14. The same as Fig. 13 but in the U_p–X plane. The initial values of X_0 are indicated near the plots alongside with the sequential moments of time.

the points corresponding to $\tau = 10$ show the values of X_0 of the trajectories. As can be seen from this figure, only the trajectories corresponding to $X_0 = 0$ and 1 approach reasonably closely the grouping points at $\tau = 10$, in agreement with Fig. 11. As in the case of Fig. 11, the monotonic convergence of trajectories along the X-axis to $X_{\lim}$ can be clearly seen.

The plots Re_p versus τ for $X_0 = 0$ and 2 are shown in Fig. 9(c) for the same trajectories as in Figs. 11–12. As can be seen in Fig. 9(c), in most cases Re_p is well above 2, and for large τ, $Re_p \to 0$, as in the cases shown in Figs. 9(a), (b).

The plots of X versus τ for the same parameters as in Fig. 7 (solid curves), except for $V_a = 60$ m/s and $V_b = 5$ m/s, are shown in Fig. 13. In this case $\beta = 2$ and no equilibrium points are expected. This agrees with the nature of trajectories shown in Fig. 13 and the corresponding figure in the (X–U_p) plane (see Fig. 14). The corresponding plots Re_p versus τ for $X_0 = 0$ and 2 in Fig. 9(d) show that the flow in this case is non-Stokesian for most of the time.

Finally, we should mention that none of the trajectories shown in Figs. 8, 10, 12 and 14 is closed, in agreement with Dulac's criterion (see Appendix B).

7. Conclusions

The general equation, describing the dynamics of spherical particles is simplified so that only the contribution of the drag force is taken into account. It is pointed out that in the case of spherical particles moving in an oscillating Stokesian flow this approximation can be justified when the host gas density is much less than the particle density and the Stokes number is not too large. In this case the contribution of inertial and added-mass forces can be ignored. This equation has been formulated in the frame of reference moving with the phase velocity of the wave and has been simplified in two limiting cases. Firstly, the case when Stokes numbers are small has been considered. Secondly, the analysis is focused on the case when the initial location of the particles, x_0, is close to the location where the particles are grouped (their velocities and accelerations in the wave frame of reference are equal to zero), $x_{\lim}$. In both cases, the analytical solutions of this equation have been obtained, investigated and validated against its numerical solutions. It is pointed out that in the first case, the solution predicts three types of trajectories depending on parameter β, defined as the ratio of the unperturbed flow velocity in the wave frame of reference and the amplitude of velocity oscillations. For $|\beta| < 1$, the particle grouping is predicted when $x = x_{\lim} = \arcsin(\beta)\lambda/(2\pi)$ and $\cos(\arcsin\beta) > 0$, where λ is the wavelength. For $|\beta| > 1$, no particle grouping is predicted. For $\beta \to \infty$ the average particle velocity is predicted to be equal to the unperturbed flow velocity. For $\beta \to +1$, this velocity approaches wave phase velocity. For $|\beta| = 1$ a one-sided grouping is predicted.

Three types of trajectories are predicted when x approaches $x_{\lim}$: monotonic approach to $x_{\lim}$; approach to $x_{\lim}$ with oscillations; and trajectories repelled from $x_{\lim}$. These are identified with stable nodes, stable foci and saddles. The trajectories in the zone between stable nodes and foci are identified as stable stars. These conclusions are shown to be valid in the general case of non-Stokesian trajectories.

Using Dulac's criterion, it is pointed out that none of the trajectories in the position-velocity plane can be closed. This result has been illustrated by the trajectories calculated using the numerical solution of the equation for particle dynamics for various parameter values.

Acknowledgements

The authors are grateful to EPSRC (Grant EP/D002044/1), UK, for their financial support.

Appendix A

For the general analysis of Solution (20) for $\beta > 1$ we assume, without loss of generality, that

$$\beta \tan\frac{X_0}{2} = 1. \tag{A.1}$$

If this is not the case from the very beginning then a point on the particle trajectory satisfying this equation can be chosen as the initial point.

Taking X_0 satisfying Eq. (A.1), Eq. (20) can be rewritten as:

$$\tan\left[\frac{\sqrt{\beta^2-1}U_b(\tau-\tau_0)}{2}\right] = \frac{\beta\tan\frac{X}{2}-1}{\sqrt{\beta^2-1}}. \tag{A.2}$$

The left and right-hand sides of this equation become infinitely large ($+\infty$) simultaneously when

$$\tau = \tau_0 + \frac{\pi(1+4n)}{U_b\sqrt{\beta^2-1}}, \tag{A.3}$$

and

$$X = \pi(1+4n). \tag{A.4}$$

In contrast to the case when $|\beta| \leqslant 1$, no grouping ($X \to X_{\lim}$ when $\tau \to \infty$) is expected for $|\beta| > 1$. This agrees with the result reported by [12], based on the numerical solution of Eq. (9).

As follows from Eqs. (A.3) and (A.4), these peaks in the values of the left and right-hand sides of Eq. (A.2) occur with the period

$$\Delta\tau = \frac{4\pi}{U_b\sqrt{\beta^2-1}} \tag{A.5}$$

over time and the period

$$\Delta X = 4\pi \tag{A.6}$$

in space.

Eqs. (A.5) and (A.6) allow us to predict the average velocity of particles in an oscillating flow given by Eq. (24).

Appendix B

Firstly, we calculate the divergence of vector $(P(X,Y), Q(X,Y))$ (see Eq. (42)) with the weighting function $St_{\rm eq}(Y)$:

$$D(X,Y) = \frac{\partial(St_{\rm eq}(Y)P(X,Y))}{\partial X} + \frac{\partial(St_{\rm eq}(Y)Q(X,Y))}{\partial Y} = -1, \tag{B.1}$$

where we took into account that $P(X,Y) = Y$ and does not explicitly depend on X.

Eq. (B.1) shows that $D(X,Y)$ is never equal to 0. Hence, using Dulac's criterion (see [32], page 130) we can expect that there is no periodic orbit which lies entirely in the (X,Y) plane. This is illustrated in Section 6 where the particle trajectories in the (X,Y) plane are calculated numerically.

System (42) has no equilibria for $b/a < 1$, which means that it has no solutions for $\dot{Y} = Y = 0$. This agrees with the results of our previous analysis, remembering that $b/a = 1/\beta$ and the condition $b/a < 1$ corresponds to our previous condition $\beta > 1$.

In the case when $b/a > 1$ system (42) has two equilibria for $X \in (0, 2\pi)$ when

$$X = X_{\rm eq} = \arcsin(a/b). \tag{B.2}$$

Since we a priori assumed that a and b are positive, we can expect that these equilibria are in the range $(0,\pi)$. Assuming that the first equilibrium $O_1(X_{\rm eq1}, 0)$ is in the range $(0, \pi/2)$, the location of the second equilibrium can be found as $O_2(\pi - X_{\rm eq1}, 0)$. Remembering that $b/a = 1/\beta$, $X_{\rm eq}$ is identical to $X_{\rm lim}$ as introduced and discussed in Section 3.

To establish the type of trajectories in the vicinity of these equilibrium points, the corresponding Jacobian matrices need to be calculated (see Section 5.1 in [32]):

$$J(X,Y)|_{X=X_{\rm eq},Y=0} = \left.\begin{pmatrix} \frac{\partial P(X,Y)}{\partial X} & \frac{\partial P(X,Y)}{\partial Y} \\ \frac{\partial Q(X,Y)}{\partial X} & \frac{\partial Q(X,Y)}{\partial Y} \end{pmatrix}\right|_{X=X_{\rm eq},Y=0}. \tag{B.3}$$

For equilibrium $O_1(X_{\rm eq1}, 0)$, expression (B.3) can be simplified to:

$$J(X,Y)|_{X=X_{\rm eq1},Y=0} = \begin{pmatrix} 0 & 1 \\ -\sqrt{b^2-a^2}/St_{\rm eq}(0) & -1/St_{\rm eq}(0) \end{pmatrix}. \tag{B.4}$$

The eigenvalues λ of this Jacobian matrix can be found from the solution of the following equation:

$$\lambda^2 + \frac{1}{St_{\rm eq}(0)}\lambda + \frac{\sqrt{b^2-a^2}}{St_{\rm eq}(0)} = 0. \tag{B.5}$$

The nature of trajectories in the vicinity of $O_1(X_{\rm eq1}, 0)$ depends on the sign of

$$F \equiv \frac{1}{St_{\rm eq}(0)^2} - 4\frac{\sqrt{b^2-a^2}}{St_{\rm eq}(0)}. \tag{B.6}$$

If $F > 0$ then both eigenvalues are real and negative and the equilibrium $O_1(X_{\rm eq1}, 0)$ is a stable node (see [32]). For the case of Stokesian trajectory this result is identical to the one obtained earlier in Section 3 (see Zone 1 in Fig. 1).

If $F < 0$ then both eigenvalues are complex with the same negative real part and the equilibrium $O_1(X_{eq1}, 0)$ is a stable focus (see [32]). For the case of Stokesian trajectory this result is identical to the one obtained earlier in Section 3 (see Zone 2 in Fig. 1).

If $F = 0$ then both eigenvalues are equal and negative. In this case the equilibrium $O_1(X_{eq1}, 0)$ is a stable star (see [32]). This corresponds to the boundary between Zones 1 and 2 in Fig. 1.

For equilibrium $O_2(X_{eq2}, 0)$, expression (B.3) can be simplified to:

$$J(X,Y)|_{X=X_{eq2},Y=0} = \begin{pmatrix} 0 & 1 \\ \sqrt{b^2-a^2}/St_{eq}(0) & -1/St_{eq}(0) \end{pmatrix}. \tag{B.7}$$

The eigenvalues λ of this Jacobian matrix can be found from the solution of the following equation:

$$\lambda^2 + \frac{1}{St_{eq}(0)}\lambda - \frac{\sqrt{b^2-a^2}}{St_{eq}(0)} = 0. \tag{B.8}$$

Eq. (B.8) has one positive and one negative root. Thus, the equilibrium $O_2(X_{eq2}, 0)$ is a saddle (see [32]). For the case of Stokesian trajectory this result is identical to the one obtained earlier in Section 3 (see Zone 3 in Fig. 1).

In the case when $b/a = 1$ system (42) has one equilibrium $O(\pi/2, 0)$. The Jacobian matrix in this case has the form:

$$J(X,Y)|_{X=\pi/2,Y=0} = \begin{pmatrix} 0 & 1 \\ 0 & -1/St_{eq}(0) \end{pmatrix}. \tag{B.9}$$

The eigenvalues λ of this Jacobian matrix can be found from the solution of the following equation:

$$\lambda^2 + \frac{1}{St_{eq}(0)}\lambda = 0. \tag{B.10}$$

Eq. (B.10) has one zero and one negative root. To establish the types of trajectories in this case, which corresponds to $\beta = 1$, further analysis of the equation is required. In this case the contribution of non-linear terms needs to be taken into account. This analysis is beyond the scope of this paper. As follows from the numerical analysis, discussed in Section 6, in this case an unstable equilibrium is expected.

References

[1] F. Kaplanski, S.S. Sazhin, Y. Rudi, Particle dynamics and mixing in an oscillating viscous pair, Proc. Estonian Acad. Sci. Eng. 11 (2) (2005) 140–153.
[2] J. Pozorski, S.S. Sazhin, M. Wacławczyk, C. Crua, D. Kennaird, M.R. Heikal, Spray penetration in a turbulent flow, Flow, Turbulence and Combustion 68 (2) (2002) 153–165.
[3] S.S. Sazhin, F. Kaplanski, G. Feng, M.R. Heikal, P.J. Bowen, A fuel spray induced vortex ring, Fuel 80 (13) (2001) 1871–1883.
[4] H. Malissa (Ed.), Analysis of Airborne Particles by Physics Methods, CRC Press, Florida, 1978.
[5] R.M. Harrison, R.E. van Grieken (Eds.), Atmospheric Particles, John Wiley & Sons, Chichester, 1998.
[6] W.H. Walton (Ed.), Inhaled Particles, vols. 1 and 2, Pergamon Press, Oxford, 1977.
[7] P. Eastwood, Critical Topics in Exhaust Gas Aftertreatment, Research Studies Press Ltd, 2000.
[8] P.F. Flynn, R.P. Durrett, G.L. Hunter, A.O. zur Loye, O.C. Akinyemi, J.E. Dec, C.K. Westbrook, Diesel combustion: an integrated view combining laser diagnostics, chemical kinetics, and empirical validation, SAE report 1999-01-0509, 1999.
[9] S.S. Sazhin, Advanced models of fuel droplet heating and evaporation, Progr. Energy Combust. Sci. 32 (2) (2006) 162–214.
[10] W.A. Sirignano, Fluid dynamics and Transport of Droplets and Sprays, Cambridge University Press, Cambridge, 1999.
[11] E.E. Michaelides, Hydrodynamic force and heat/mass transfer from particles, bubbles, and drops – the Freeman scholar lecture, ASME J. Fluid Engrg. 125 (2003) 209–238.
[12] D. Katoshevski, Z. Dodin, G. Ziskind, Aerosol clustering in oscillating flows: mathematical analysis, Atomization and Sprays 15 (2005) 401–412.
[13] F. Mashayek, R.V.R. Pandya, Analytical description of particle laden flows, Progr. Energy Combust. Sci. 29 (2003) 329–378.
[14] Y.D. Afanasyev, V.N. Korabel, Starting vortex dipoles in a viscous fluid: asymptotic theory, numerical simulation, and laboratory experiments, Phys. Fluids 16 (11) (2004) 3850–3858.
[15] F. Kaplanski, Y. Rudi, A model for the formation of 'optimal' vortex rings taking into account viscosity, Phys. Fluids 17 (2005) 087101.
[16] D.R. Poole, C.F. Barenghi, Y.A. Sergeev, W.F. Vinen, The motion of tracer particles in helium II, Phys. Rev. B 71 (2005), 064514-1-16.
[17] C.F.M. Coimbra, M.H. Kobayashi, On the viscous motion of a small particle in a rotating cylinder, J. Fluid Mech. 469 (2002) 257–286.
[18] R.L. Panton, Incompressible Flow, second ed., John Wiley & Sons, New York, Chichester, 1996.
[19] M.R. Maxey, J.J. Riley, Equation of motion for a small rigid sphere in a nonuniform flow, Phys. Fluids 26 (4) (1983) 883–889.

[20] T.R. Auton, J.C.R. Hunt, M. Prud'homme, The force exerted on a body in inviscid unsteady non-uniform rotational flow, J. Fluid Mech. 197 (1988) 241–257.
[21] R. Mei, Flow due to an oscillating sphere and an expression for unsteady drag on the sphere at finite Reynolds number, J. Fluid Mech. 270 (1994) 133–174.
[22] I. Kim, S. Elghobashi, W.A. Sirignano, On the equation for spherical-particle motion: effect of Reynolds and acceleration numbers, J. Fluid Mech. 367 (1998) 221–253.
[23] S.S. Sazhin, Whistler-Mode Waves in a Hot Plasma, Cambridge University Press, Cambridge, 1993.
[24] M. Abramovitz, I.A. Stegun, Handbook of Mathematical Functions, National Bureau of Standards, USA, 1964.
[25] G.A. Korn, T.M. Korn, Mathematical Handbook, McGraw-Hill, New York, 1968.
[26] S.S. Sazhin, G. Feng, M.R. Heikal, A model for fuel spray penetration, Fuel 80 (15) (2001) 2171–2180.
[27] S.S. Sazhin, C. Crua, D. Kennaird, M.R. Heikal, The initial stage of fuel spray penetration, Fuel 82 (8) (2003) 875–885.
[28] E.M. Sazhina, S.S. Sazhin, M.R. Heikal, V.I. Babushok, R. Johns, A detailed modelling of the spray ignition process in Diesel engines, Combust. Sci. Technol. 160 (2000) 317–344.
[29] J.D. Hoffman, Numerical Methods for Engineers and Scientists, second ed., Marcel Dekker, New York, 2001.
[30] J.H. Seinfeld, S.N. Pandis, Atmospheric Chemistry and Physics – From Air Pollution to Climate Change, John Wiley & Sons, 1997.
[31] A.A. Andronov, A.A. Witt, S.E. Khaikin, Theory of Oscillators, Pergamon Press, 1966.
[32] P. Glendinning, Stability, Instability and Chaos, Cambridge University Press, Cambridge, 1996.